Supplemental Information for

Surface-Sensitive Spectrometry: New Insights into Radical Reactions at Interfaces

Zachary R. Schiffman[1], Yuekun Yang[1], Barbara J. Finlayson-Pitts[1] and Lisa M. Wingen[1]*

[1]*Department of Chemistry, University of California, Irvine, Irvine, California 92697, USA*

*Email: *wingenit@uci.edu*

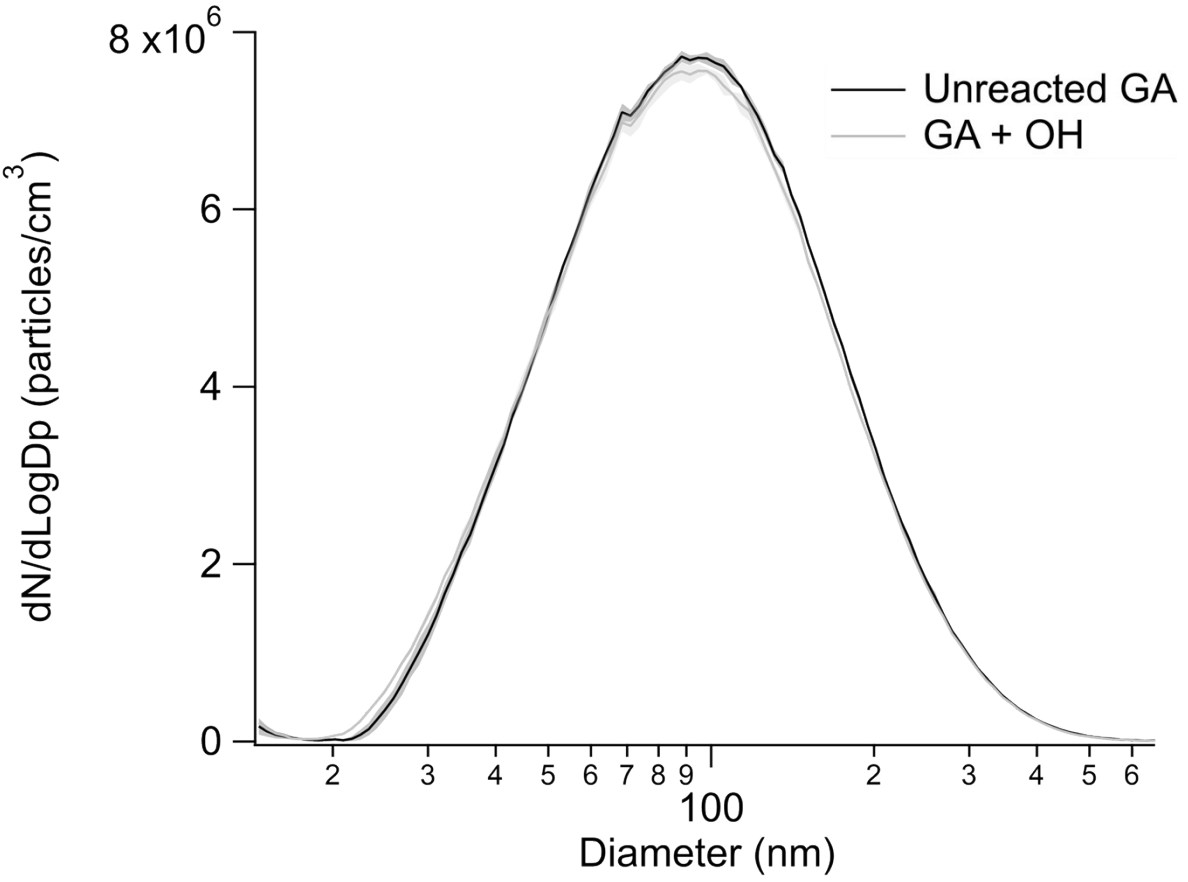

Figure S1. Typical size distributions of atomized and dried GA particles before (black) and after (gray) reaction with OH radicals (0.9 ppm TME and 7.5 ppm ozone) as measured with a scanning mobility particle sizer (SMPS). The GA concentration in the atomizer was 20 mM. Each distribution is an average of five scans ± one standard deviation.

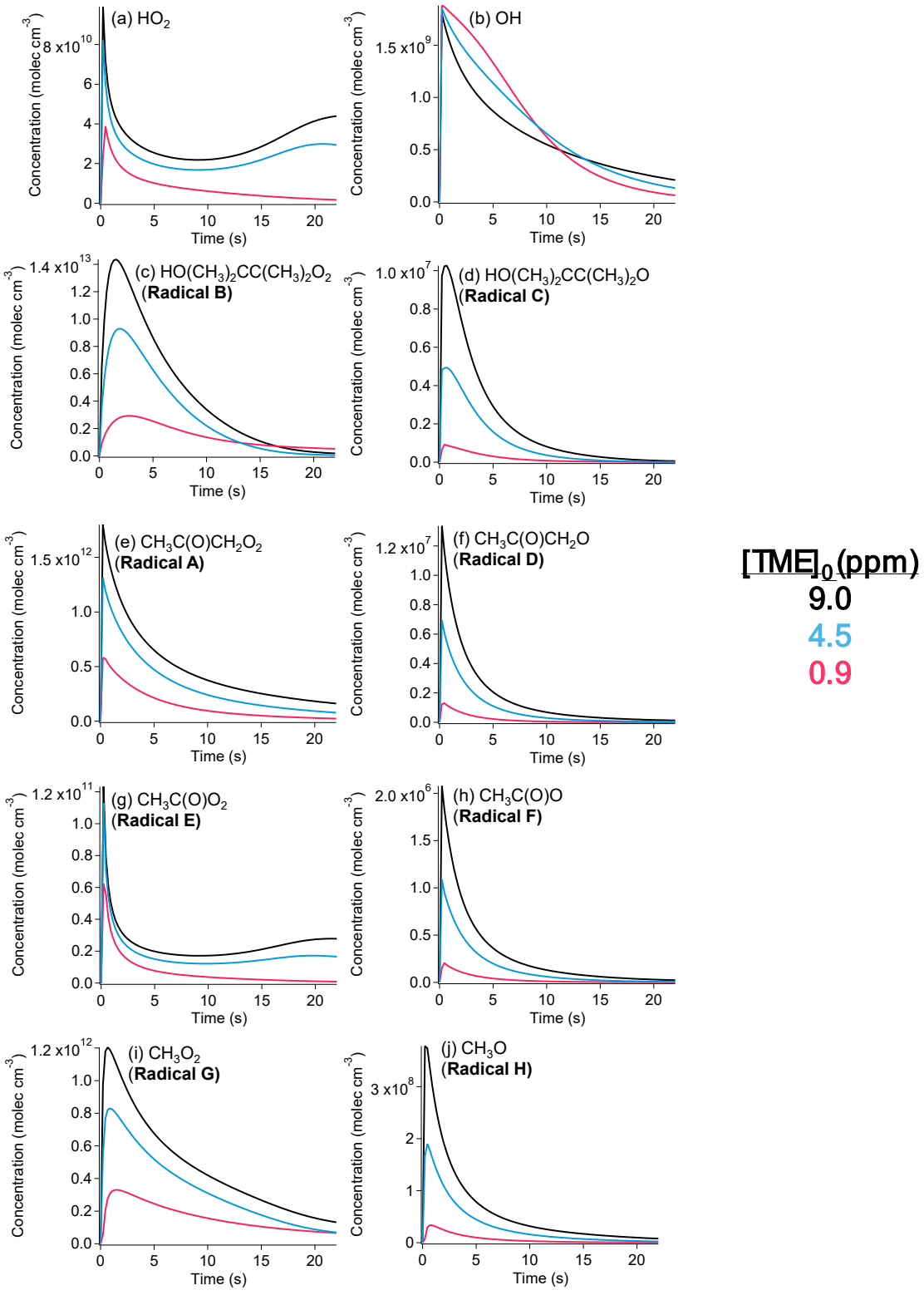

24

25 **Figure S2**. Examples of output from the KinSim model of gas-phase radicals for initial
26 conditions of 7.5 ppm O_3 and variable $[TME]_0$ in air. (a) HO_2; (b) OH; (c) Radical B = hydroxy-

TME-peroxy = $HO(CH_3)_2CC(CH_3)_2O_2$; (d) Radical C = hydroxy-TME-alkoxy = $HO(CH_3)_2CC(CH_3)_2O$; (e) Radical A = acetonyl peroxy = $CH_3C(O)CH_2O_2$; (f) Radical D = acetonyl alkoxy = $CH_3C(O)CH_2O$; (g) Radical E = acetyl peroxy = $CH_3C(O)O_2$; (h) Radical F = acetyl alkoxy = $CH_3C(O)O$; (i) Radical G = methyl peroxy = CH_3O_2; (j) Radical H = methyl alkoxy = CH_3O.

Table S1. The reactions used in the KinSim model including rate constants.

Reactant 1	(Reactant 2)	Product 1	(Product 2)	(Product 3)	k (cm^3 $molec^{-1}$ s^{-1})[a]
Acetol	OH	Methylglyoxal	HO_2		4.45E-12[b]
Acetone	OH	$CH_3C(O)CH_2O_2$			1.75E-13 [b]
$CH_3C(O)CH_2O$		$CH_3C(O)O_2$	Formaldehyde		1.00E06 [b]
$CH_3C(O)CH_2O_2$	CH_3O_2	$CH_3C(O)CH_2O$	CH_3O	O_2	1.10E-12[c]
$CH_3C(O)CH_2O_2$	CH_3O_2	MeOH	Methylglyoxal	O_2	1.90E-12 [c]
$CH_3C(O)CH_2O_2$	CH_3O_2	Formaldehyde	Acetol	O_2	7.60E-13 [c]
$CH_3C(O)CH_2O_2$	HO_2	$CH_3C(O)CH_2O$	OH		1.35E-12 [b]
$CH_3C(O)CH_2O_2$	HO_2	$CH_3C(O)CH_2OOH$			7.67E-12 [b]
$CH_3C(O)CH_2O_2$	$HO(CH_3)_2CC(CH_3)_2O_2$	$CH_3C(O)CH_2O$	$HO(CH_3)_2CC(CH_3)_2O$		3.22E-14 [b,j]
$CH_3C(O)CH_2O_2$	$HO(CH_3)_2CC(CH_3)_2O_2$	Pinacol[h]	Methylglyoxal		1.38E-14 [b,j]
$CH_3C(O)CH_2O_2$	$CH_3C(O)CH_2O_2$	$CH_3C(O)CH_2O$	$CH_3C(O)CH_2O$	O_2	1.58E-12 [d]
$CH_3C(O)CH_2O_2$	$CH_3C(O)CH_2O_2$	Methylglyoxal	Acetol		3.22E-12 [d]
$CH_3C(O)CH_2OOH$	OH	$CH_3C(O)CH_2O_2$			3.59E-12 [b]
Acetic acid	OH	CH_3O_2			8.00E-13 [b]
$CH_3C(O)O$	O_2	CO_2	CH_3O_2		1.20E-12 [b]
$CH_3C(O)O_2$	$CH_3C(O)O_2$	$CH_3C(O)O$	CH_3COO	O_2	1.30E-11[e]
$CH_3C(O)O_2$	CH_3O_2	$CH_3C(O)O$	CH_3O	O_2	1.30E-11 [e]
$CH_3C(O)O_2$	CH_3O_2	Acetic acid	Formaldehyde	O_2	6.50E-12 [e]
$CH_3C(O)O_2$	$CH_3C(O)CH_2O_2$	$CH_3C(O)O$	$CH_3C(O)CH_2O$		2.50E-12 [c]
$CH_3C(O)O_2$	$CH_3C(O)CH_2O_2$	Acetic acid	Methylglyoxal	O_2	2.50E-12 [c]
$CH_3C(O)O_2$	HO_2	Acetic acid	O_3		9.10E-12 [b]
$CH_3C(O)O_2$	HO_2	$CH_3C(O)OOH$	O_2		3.90E-12 [b]
$CH_3C(O)O_2$	$HO(CH_3)_2CC(CH_3)_2O_2$	$CH_3C(O)O$	$HO(CH_3)_2CC(CH_3)_2O$		1.10E-11[f,j]
$CH_3C(O)OOH$	OH	$CH_3C(O)O_2$			3.70E-12 [b]
CO	OH	HO_2			2.28E-13 [b]
Criegee		$CH_3C(O)CH_2O_2$	OH		1.00E06 [b]
Formaldehyde	OH	HO_2	CO		8.49E-12 [b]
H	HO_2	H_2	O_2		5.60E-12 [b]
H	HO_2	OH	OH		7.20E-11 [b]
H	HO_2	H_2O	O		2.40E-12 [b]
H	O_2	HO_2			1.00E-12 [b]
HO_2	HO_2	H_2O_2	O_2		1.60E-12 [b]
HO_2	O_3	OH	O_2	O_2	2.00E-15 [b]
Methylglyoxal	OH	H_2O	$CH_3C(O)O_2$	CO	7.85E-12 [b]
Methylglyoxal	OH	CO	CO	CH_3O_2	5.23E-12 [b]
CH_3O	O_2	HO_2	Formaldehyde		2.00E-15 [b]

CH_3O_2	HO_2	CH_3OOH			4.74E-12 [b]
CH_3O_2	HO_2	Formaldehyde			4.67E-13 [b]
CH_3O_2	CH_3O_2	CH_3O	CH_3O	O_2	1.20E-13 [f]
CH_3O_2	CH_3O_2	MeOH	Formaldehyde	O_2	2.40E-13 [f]
CH_3O_2	$HO(CH_3)_2CC(CH_3)_2O_2$	CH_3O	$HO(CH_3)_2CC(CH_3)_2O$		4.00E-16 [f,j]
CH_3O_2	$HO(CH_3)_2CC(CH_3)_2O_2$	Pinacol	Formaldehyde		2.70E-15 [f,j]
MeOH	OH	HO_2	Formaldehyde		8.95E-13 [b]
CH_3OOH	OH	Formaldehyde	OH		6.02E-12 [b]
CH_3OOH	OH	CH_3O	OH		4.01E-12 [b]
O	O_2 +M	O_3 +M			1.40E-14 [g]
O	O_3	O_2	O_2		8.00E-15 [g]
O	OH	O_2	H		3.50E-11 [g]
O	HO_2	OH	O_2		5.80E-11 [g]
O	H_2O_2	OH	HO_2		1.70E-15 [g]
OH	H_2	H_2O	H		6.70E-15 [g]
OH	OH	H_2O	O		1.48E-12 [g]
OH	OH	H_2O_2			6.20E-12 [g]
OH	HO_2	H_2O	O_2		1.10E-10 [g]
OH	H_2O_2	H_2O	HO_2		1.70E-12 [g]
OH	O_3	HO_2	O_2		7.30E-14 [g]
TME	O_3	Acetone	Criegee		1.13E-15 [b]
TME	OH	OH-TME-O_2			1.10E-10 [b]
OH-TME-O_2	O_2	$HO(CH_3)_2CC(CH_3)_2O_2$			1.00E06 [b]
$HO(CH_3)_2CC(CH_3)_2O$		Acetone	Acetone	HO_2	1.00E06 [b]
$HO(CH_3)_2CC(CH_3)_2O_2$	HO_2	$HO(CH_3)_2CC(CH_3)_2OOH$			1.76E-11 [b,j]
$HO(CH_3)_2CC(CH_3)_2O_2$	$HO(CH_3)_2CC(CH_3)_2O_2$	$HO(CH_3)_2CC(CH_3)_2O$	$HO(CH_3)_2CC(CH_3)_2O$		5.70E-15 [b,j]
Pinacol	OH	$HO(CH_3)_2CC(CH_3)_2O$			9.49E-13 [b]
$HO(CH_3)_2CC(CH_3)_2OOH$	OH	$HO(CH_3)_2CC(CH_3)_2O_2$			4.40E-12 [b]
OH	Glutaric Acid	Ox Products			2.11[i]

[a] This unit for rate constant applies only to bimolecular reactions. For a unimolecular reaction, the unit for rate constant is s^{-1}.
[b] Master Chemical Mechanism[1,2]
[c] Atkinson et al. 2006[3]
[d] Zuraski et al. 2023[4]
[e] Assali et al. 2022[5]
[f] Villenave et al. 1998[6]
[g] Atkinson et al. 2004[7]
[h] Pinacol is 2,3-dimethylbutane-2,3-diol
[i] See Text S1

[j] Rate constants used here for the reaction of the hydroxy-TME radicals are based on the reactions of the *t*-butyl peroxy radical as suggested by Jenkin et al.[8]

Text S1. *Calculation of Collision Rates and Related Discussion*.

To examine the effect that the particle surfaces play on the modeled OH concentrations, the collision rate between GA particles and the gas-phase OH radical as a function of surface area is calculated. Only the particle surface is considered here as a sink for gaseous OH and the model does not consider surface depletion. The rate of reaction of OH with the surface ($cm^{-3}\ s^{-1}$) is given by eq. S1,

$$Rate = Z \times (SA) \times \gamma = k\,[OH] \qquad \text{(S1)}$$

where k (s^{-1}) is the pseudo-first order rate constant for the reaction of OH with GA and Z is the number of collisions per second per unit surface area, defined in Equation S2:

$$Z = \frac{Collisions}{cm^2 * s} = [OH]\sqrt{\frac{RT}{2\pi M}} \times \frac{100\ cm}{m} \qquad \text{(S2)}$$

SA is the surface area concentration in cm^2 per cm^3 air as measured by SMPS; γ is the probability of a collision leading to a loss of OH through reaction; and [OH] is the number concentration of OH radicals in molecules cm^{-3}. R is the ideal gas law constant (J/mol K); T is room temperature (K); and M is the molecular weight of the gas species (kg/mol).[9]

From Equations S1 and S2 the rate constant k is given by:

$$k = \sqrt{\frac{RT}{2\pi M}} \times \frac{100\ cm}{m} \times (SA) \times \gamma \qquad \text{(S3)}$$

The value of γ is estimated from the gas-phase rate constant of OH with alkanes of similar number of carbons (~5×10^{-12} cm^3 $molecule^{-1}$) relative to a collision-controlled value of ~1×10^{-10} cm^3 $molecule^{-1}$ s^{-1}. Using a value of 0.05 for γ, values for k can be estimated as summarized in Table S2. Varying the KinSim model rate constant between the minimum and maximum surface areas resulted in negligible change in modeled OH concentrations. This is expected since the major loss process for OH is reaction with TME. As such, a mean value 2.1 s^{-1} is used in the model.

Table S2. Estimated rate constants k and average OH concentrations for the reaction OH → Products as surface area concentrations are varied at 0.9 ppm TME and 7.5 ppm O_3.

GA Aqueous Concentration (mM)	Particle Surface Area Concentration (nm^2/cm^3)	k (s^{-1})	$[OH]_{avg}$ (cm^{-3})
10	1.2×10^{11}	0.86	7.2×10^{8}
20	2.5×10^{11}	1.8	7.2×10^{8}
40	3.6×10^{11}	2.6	7.2×10^{8}
60	4.2×10^{11}	3.1	7.2×10^{8}

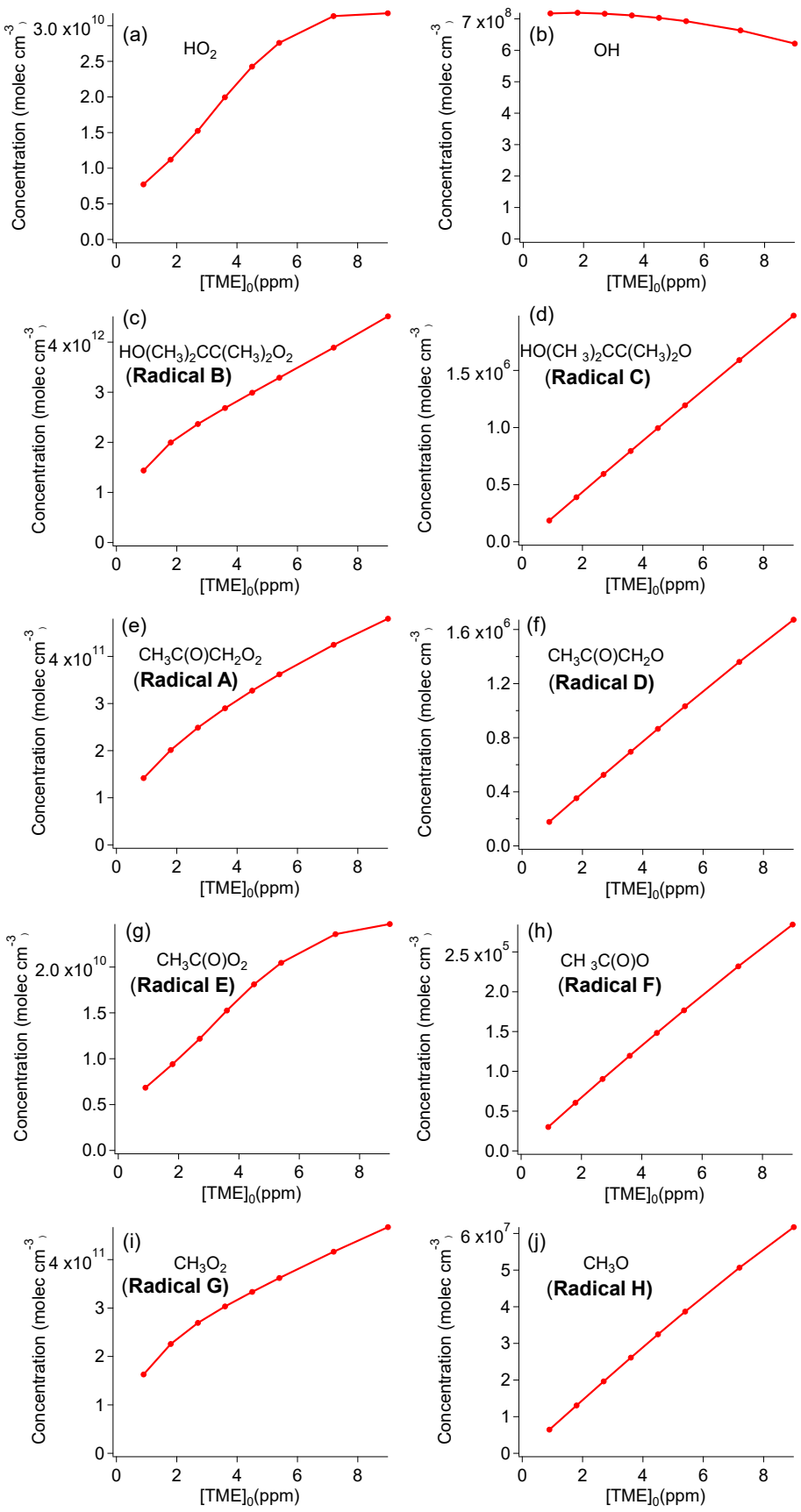
(a)
HO2
3.0 x10^10
(b)
OH
7 x10^8
(c)
HO(CH3)2CC(CH3)2O2
(Radical B)
4 x10^12
(d)
HO(CH 3)2CC(CH3)2O
(Radical C)
1.5 x10^6
(e)
CH3C(O)CH2O2
(Radical A)
4 x10^11
(f)
CH3C(O)CH2O
(Radical D)
1.6 x10^6
(g)
CH3C(O)O2
(Radical E)
2.0 x10^10
(h)
CH 3C(O)O
(Radical F)
2.5 x10^5
(i)
CH3O2
(Radical G)
4 x10^11
(j)
CH3O
(Radical H)
6 x10^7
Concentration (molec cm-3)
[TME]0(ppm)

Figure S3. The 22-second predicted average concentration of gas-phase radicals as a function of $[TME]_0$ are shown, for initial conditions of 7.5 ppm O_3 and variable $[TME]_0$ in air. (a) HO_2; (b) OH; (c) Radical B = hydroxy-TME-peroxy = $HO(CH_3)_2CC(CH_3)_2O_2$; (d) Radical C = hydroxy-TME-alkoxy = $HO(CH_3)_2CC(CH_3)_2O$; (e) Radical A = acetonyl peroxy = $CH_3C(O)CH_2O_2$; (f) Radical D = acetonyl alkoxy = $CH_3C(O)CH_2O$; (g) Radical E = acetyl peroxy = $CH_3C(O)O_2$; (h) Radical F = acetyl alkoxy = $CH_3C(O)O$; (i) Radical G = methyl peroxy = CH_3O_2; (j) Radical H = methyl alkoxy = CH_3O.

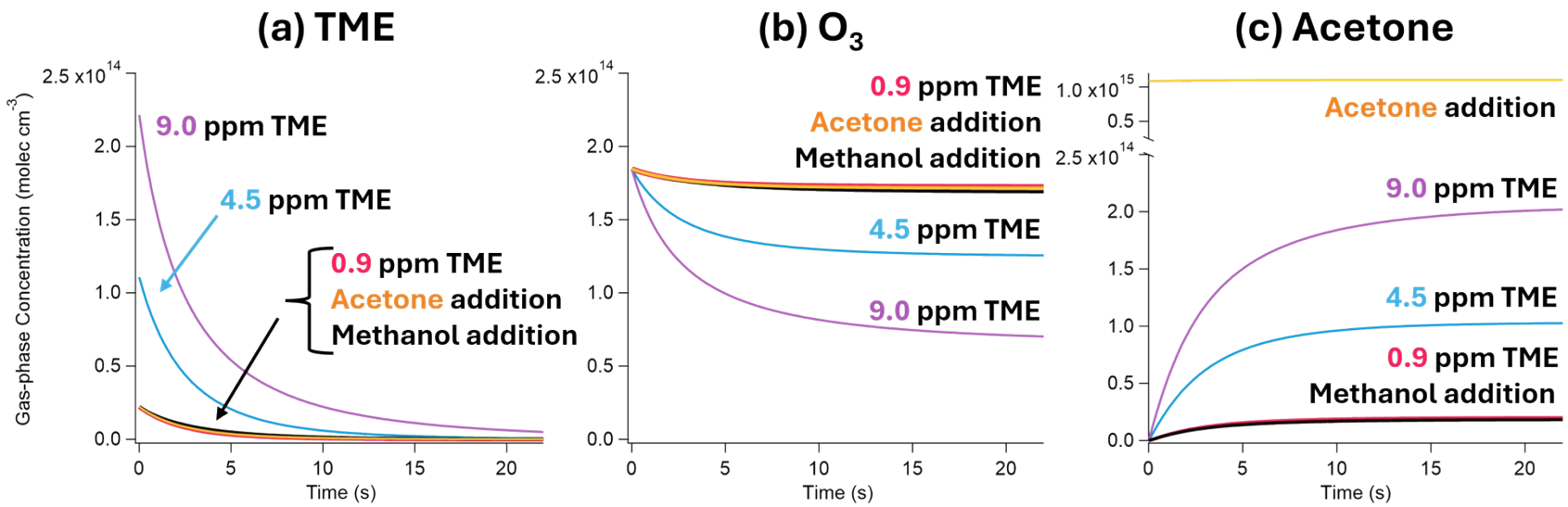

Figure S4. Time series of **(a)** TME, **(b)** ozone, and **(c)** acetone concentrations from the KinSim model for different initial conditions of 7.5 ppm O_3 and $[TME]_0$ of 0.9 (red), 4.5 (blue), and 9.0 (purple) ppm, as well as with additions of 44 ppm acetone (orange) or 53 ppm methanol (black). $[TME]_0$ is 0.9 ppm except where otherwise noted.

Text S2. *Offline UHPLC-HESI-HRMS Analysis of GA*

Unreacted glutaric acid was examined for impurities using offline ultra-high-pressure liquid chromatography with heated electrospray ionization and high-resolution mass spectrometry (UHPLC-HESI-HRMS, Thermo Fisher Scientific, Vanquish UHPLC, Q Exactive Plus orbitrap). The instrument and technique have been described in detail previously.[10] Briefly, 10 μL of an aqueous GA solution (240 μg/mL) were injected onto a Polar C18 column (Phenomenex, Luna Omega 1.6 μm Polar C18, 150 x 2.1 mm) at 30°C with a mobile phase of solvent A, 0.1% formic acid (Sigma Aldrich, 98+%) in water (Nanopure, 18.2 MΩ cm) and B, 0.1% formic acid in acetonitrile (Fisher, Optima LC-MS grade). A gradient elution was used beginning at 95% solvent A which linearly decreased to 5% A at a rate of 6.4%/min. GA was used from the manufacturer without further purification.

Additional LC-MS analysis was carried out on unreacted or oxidized GA particles that had been atomized, dried, and passed through the flow tube and were collected on PTFE filters (Fluoropore 0.2 μm) with the aid of a pump (SKC, Leland Legacy) placed downstream of the filter. Collected particles were extracted using water or deuterium oxide. The mass spectra of unreacted GA showed no difference before and after atomization, indicating no changes in the surface composition of GA due to the atomization process.

Text S3. *Discussion of Experiments to Determine the Identity of* m/z *189.*

In the previous study,[10] the peak at *m/z* 189 was tentatively assigned to a tricarboxylic acid formed from the reaction of a GA alkyl R radical with a second alkyl radical, a radical decomposition product of a GA RO radical, based on high-resolution mass measurements which revealed an elemental formula of $C_7H_{10}O_6$. However, results from this study indicate that the formation of the product at *m/z* 189 appears to vary as gas-phase radical concentrations are changed, and as such the identity and formation mechanism of this product are revisited here.

To confirm that the species at *m/z* 189 (MW 190) arises from GA oxidation rather than exclusively from reaction of gas-phase species that condense on the GA, an experiment was conducted using 3-methylglutaric acid (3-MGA) in place of GA as the matrix particle. Upon OH oxidation, analogous oxidation products of 3-MGA were observed, including the ROH (*m/z* 161*)*, R=O (*m/z* 159), and ROOH (*m/z* 177) species (Figure S5). Of note, a peak at *m/z* 189 was absent, and instead a peak at *m/z* 203 appeared, consistent with the addition of the $-CH_3$ group substituent in 3-MGA. This peak at *m/z* 203 increases with increased $[TME]_0$, just as *m/z* 189 does in the spectrum of oxidized GA. If a product had formed solely in the gas phase and condensed on the surface of the matrix particle, it would be observed in the MAIV mass spectra at the same *m/z* regardless of matrix particle. As such, the mass shift suggests that the product seen at *m/z* 189 in the oxidation of GA must incorporate a GA molecule.

To further rule out whether *m/z* 189 was formed exclusively through gas-phase chemistry (*i.e.*, through accretion reactions of TME oxidation products), an experiment was performed in which TME and ozone were allowed to react inside the flow tube in the absence of GA particles, forming gas-phase products. GA matrix particles were then added at the end of the flow tube before entering the mass spectrometer. Resulting MAIV mass spectra revealed no products

which had condensed onto particles, including at *m/z* 189. From this it is concluded that the peak observed at *m/z* 189 in the OH oxidation of GA is likely not produced in the gas phase.

It is also noted that the mass of 190 corresponds to the mass of GA (132) plus that of acetone (58). Because acetone is produced in high quantities during the ozonolysis of TME (Figure S4), experiments were performed to rule out whether *m/z* 189 is an adduct or complex between GA and acetone. First, an experiment was performed in which GA particles were exposed to high concentrations of acetone in the flow tube, in the absence of OH radicals. In addition, in order to observe whether exposure to OH radicals had disrupted the surface of particles sufficiently to encourage acetone adducts to form on the oxidized particle surface, oxidation of GA was performed in the flow tube followed by a denuder placed at the end of the flow tube. Acetone was then added after the denuder before particles entered the mass spectrometer. Because the denuder removed gas-phase oxidants including OH radicals and ozone, any increase of intensity at *m/z* 189 would necessarily be produced by adducts between acetone and the oxidized particle, rather than by gas-phase species products by the oxidation of acetone. The addition of acetone after the denuder produced no appreciable increase in *m/z* 189. As such, the acetone adduct was ruled out.

MS/MS spectra were collected to observe fragmentation of the product at *m/z* 189 (Figure S6). Collection was performed in negative ion mode with collision energy (CE) ranging between 2 and 20 eV. Major daughter ions were observed at *m/z* 131 and 75, with later daughters at higher CE at *m/z* 113, 87, and 69. *m/z* 131 is believed to be an isomer of deprotonated GA, as daughters at *m/z* 113, 87, and 69 are previously reported daughters of GA with losses of H_2O, CO_2, or $H_2O + CO_2$ respectively.[11] At this time, the identity of the daughter ion at *m/z* 75 is not known. However, the molecular identity of *m/z* 75 was additionally verified using MS/MS fragmentation in high-

resolution Orbitrap LC-MS, which revealed a formula of $[C_2H_3O_3]^-$. Possible identities for this ion include glycolate ($HOCH_2C(O)O^-$) or peracetate ($CH_3C(O)OO^-$).

Finally, in order to confirm the molecular formula and exact mass of the product, oxidized GA particles were collected on filters under conditions of both low and high TME. UHPLC-HESI-HRMS was performed on the resulting collected particles, the method of which is discussed above in Text S2. The high-resolution analysis of oxidation products revealed a product at m/z 189.0304 (53 ppm error from the exact mass of $[C_7H_9O_6]^-$), which increased by 22-fold when comparing high vs low TME conditions.

In order to provide additional information on the structure of this product MAIV-MS experiments were performed atomizing a GA solution dissolved in D_2O rather than H_2O. By doing so, labile hydrogens in product structures such as those involved with O-H bonds are able to exchange with deuterium, thus shifting the observed *m/z* value in MAIV spectra by the number of potential exchange sites. Only partial deuteration was observed from products in the MAIV spectra, as MAIV-MS is a technique performed in ambient air and likely cannot avoid reversible exchange with protonated water vapor in indoor air. However, in the deuterated spectra, a peak at *m/z* 190 is present which is not present in protonated spectra (Figure S7). From this, it can be concluded that the product at *m/z* 189 has no more than two labile hydrogens, matching the proposed structure of R"(O)OR (Scheme S1).

From these experiments a structure and formation mechanism are proposed here which produce the ester R"(O)OR from the reaction of Radical A and the GA $RO_{2(surf)}$ (Scheme S1). It has been suggested that ether and ester accretion products can form between complexed RO radicals, one of which undergoes decomposition and results in the formation of a C-O bond.[12,13] The acetonyl

171 radicals A and D increase as initial TME concentration increases (Figure S2), and thus may result
172 in increased formation of the product at *m/z* 189 as observed.

173

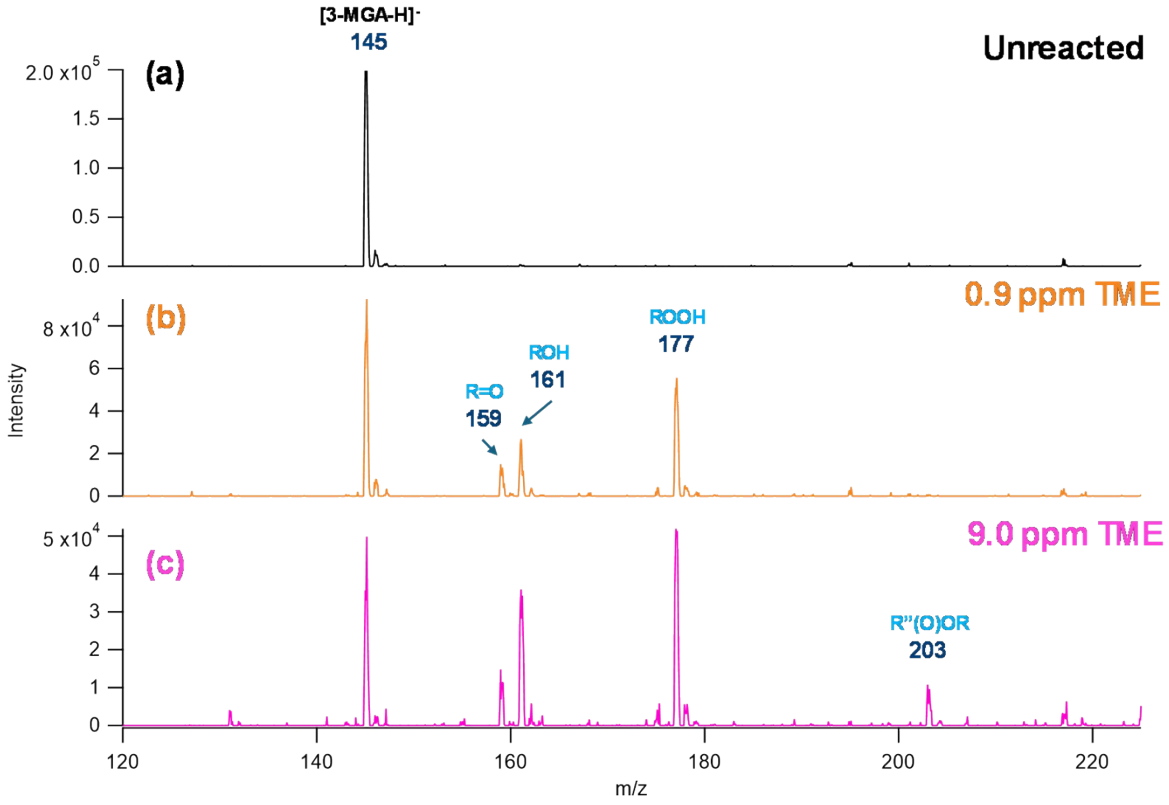

174

175

176 **Figure S5.** MAIV spectra of 3-MGA particles in negative ion mode. **(a)** unreacted 3-MGA
177 particles (black); **(b-c)** 3-MGA particles reacted with OH radicals at initial conditions of 7.5 ppm
178 ozone and (**b**) 0.9 ppm TME; **(c)** 9.0 ppm TME.

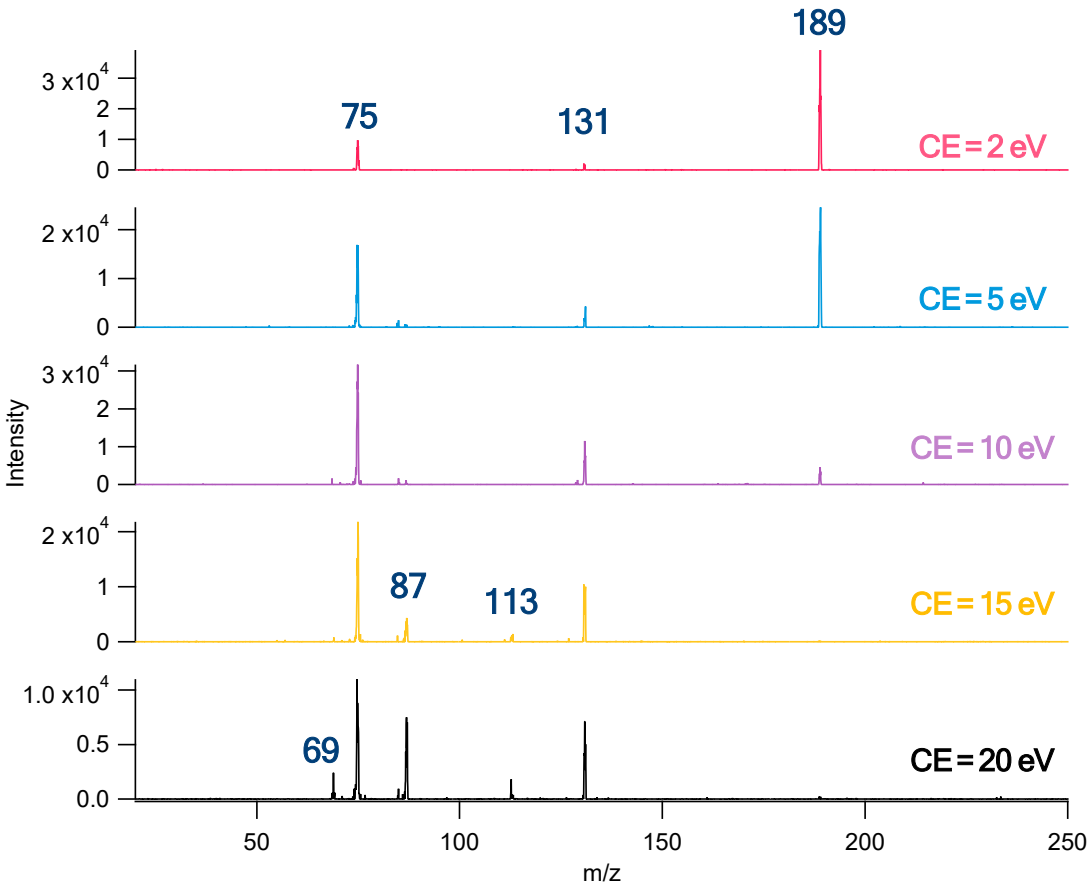

179

180 **Figure S6.** MS/MS spectra of *m/z* 189 in negative ion mode. Oxidation was performed in flow
181 tube apparatus using GA particles reacted with 10.8 ppm TME and 7.5 ppm ozone.

182

183

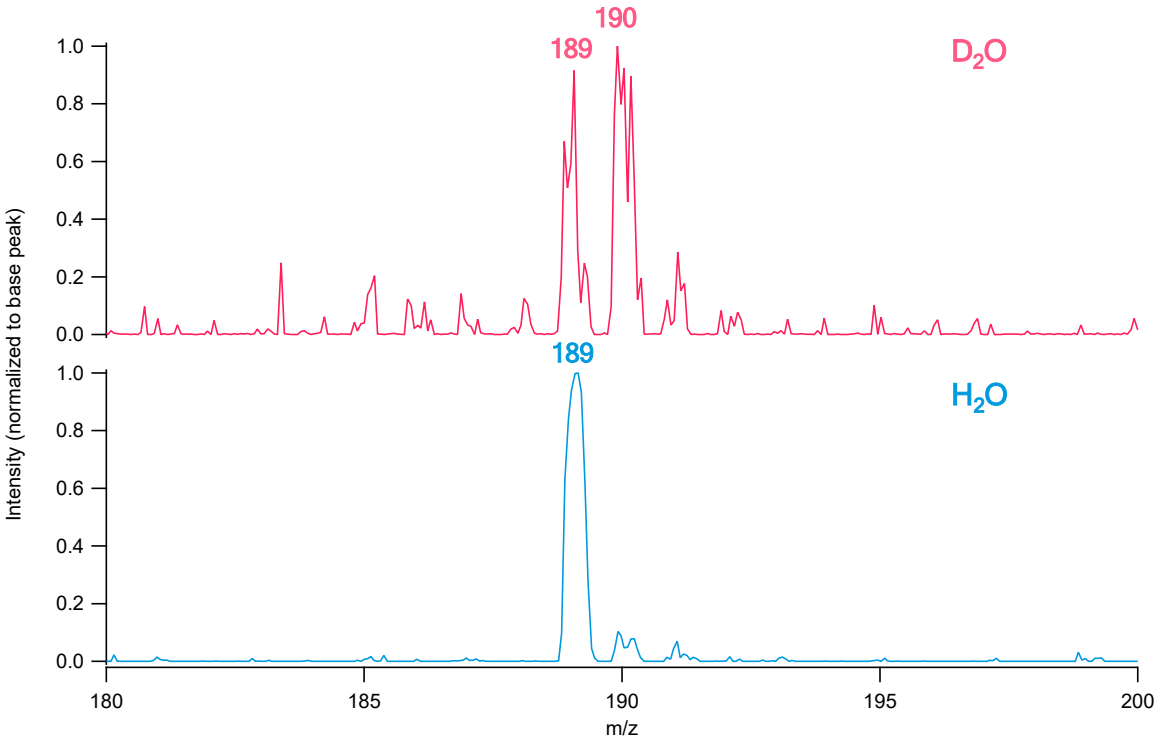

184

185 **Figure S7.** MAIV spectra of GA particles in negative ion mode after reaction with OH radicals
186 at 9.0 ppm TME + 7.5 ppm ozone. Spectra of GA particles **(top)** dissolved in D_2O; and **(bottom)**
187 dissolved in H_2O. [R"(O)OR – H]$^-$, *m/z* 189; [R"(O)OR_D – D]$^-$, *m/z* 190. Peak intensities are
188 normalized to the base peaks.

189

190

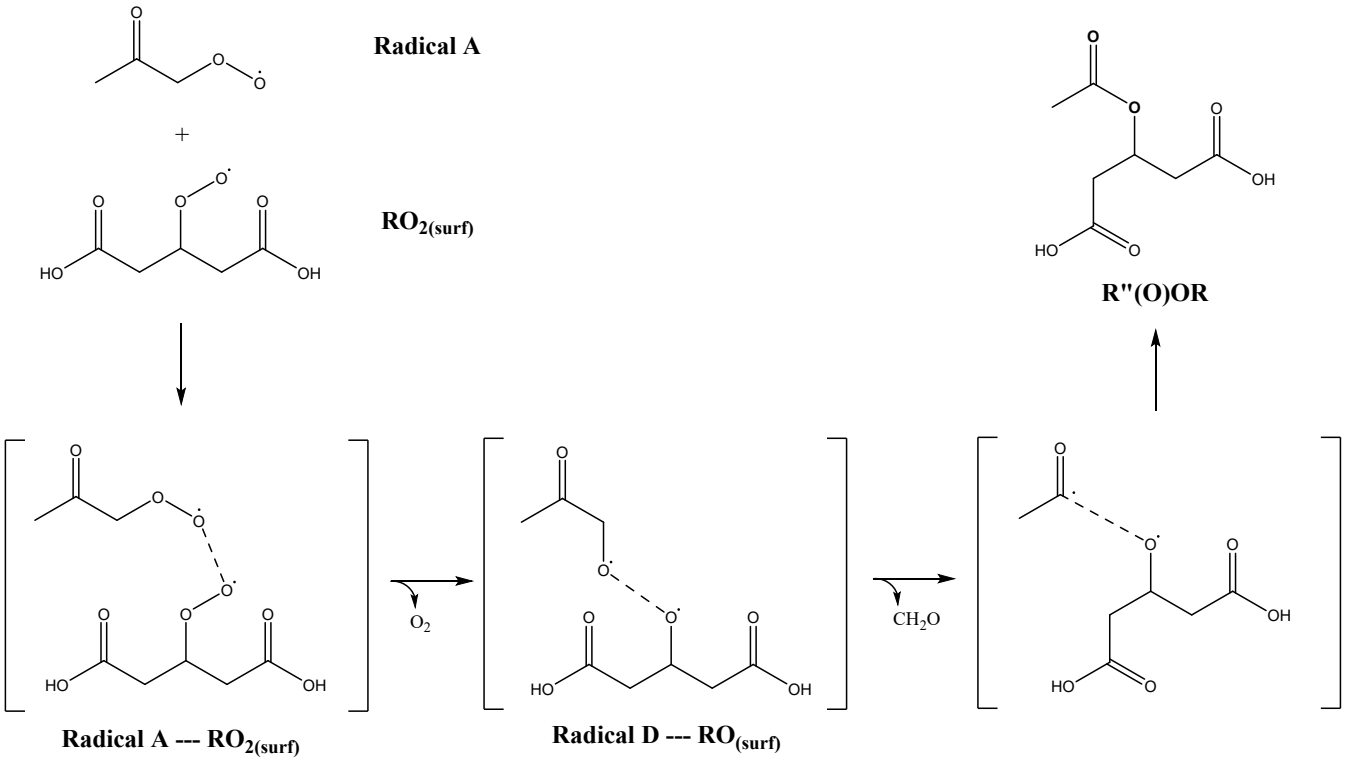

Scheme S1. Suggested formation mechanisms for an ester (R''(O)OR) of molecular weight 190.

Text S4. *Observation of Hydrogen-Deuterium Exchange using HESI-HRMS.*

Oxidized GA particles (0.9 ppm TME and 7.5 ppm O_3) after filter collection were extracted using D_2O (deuterium oxide, for NMR, Thermo Scientific, 99.8% atom D) instead of H_2O and examined using offline Orbitrap HESI-HRMS**.** Samples were directly injected into the HESI inlet to avoid protonation from the protic eluent used in UHPLC. Species which possess labile hydrogen sites (*i.e.,* O-H bonds) will undergo hydrogen-deuterium exchange when dissolved in D_2O. As such, the products in the resulting mass spectra will undergo a shift of *m/z* depending on the number of labile sites. Because ions in negative mode are observed as $[M\text{-}D]^-$, deuterated peaks will shift +1 *m/z* for each labile hydrogen not including one carboxylic acid site.

The HESI-HRMS mass spectrum reveals the presence of three major products from GA oxidation, including two expected oxidation products as well as one additional product (Figure S8). The peaks for the R=O and ROD products appear where expected: R=O is seen at *m/z* 146, shifted +1 from its single acid group, and ROD is seen at *m/z* 149, shifted +2 from its acid group and hydroxyl group. The ROOD species (*m/z* 165) is not observed as a significant product in Orbitrap MS, which is expected due to the fragility of peroxide bonds in the harsh conditions of the electrospray ionization.[10] However, a product at *m/z* 166 is observed, consistent with a diol $R(OD)_2$ which shifts +3 from its acid group and two hydroxyl groups.

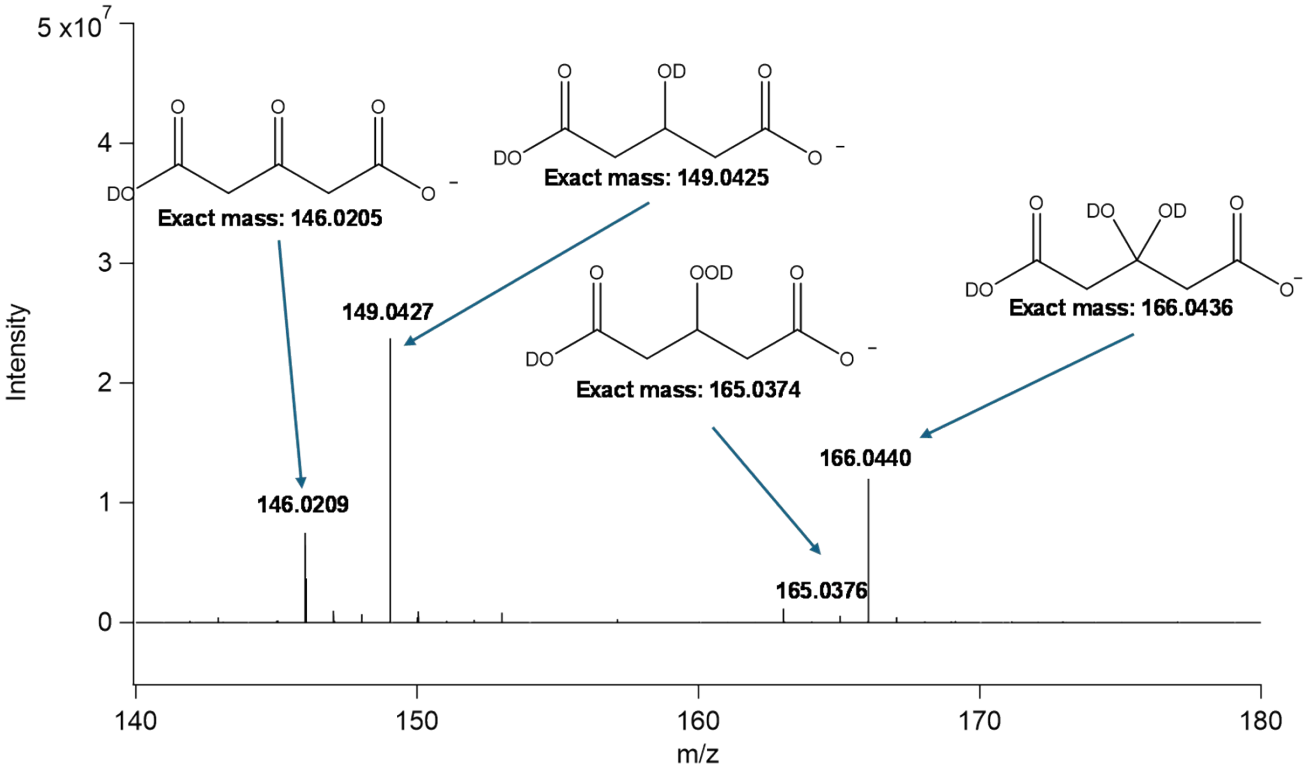

Figure S8. High-resolution mass spectrum obtained from HESI-Orbitrap direct injection of oxidized GA particles extracted in D_2O (9.0 ppm TME and 7.5 ppm O_3). All accurate mass measurements were within 2.6 ppm error of exact masses for the structures provided.

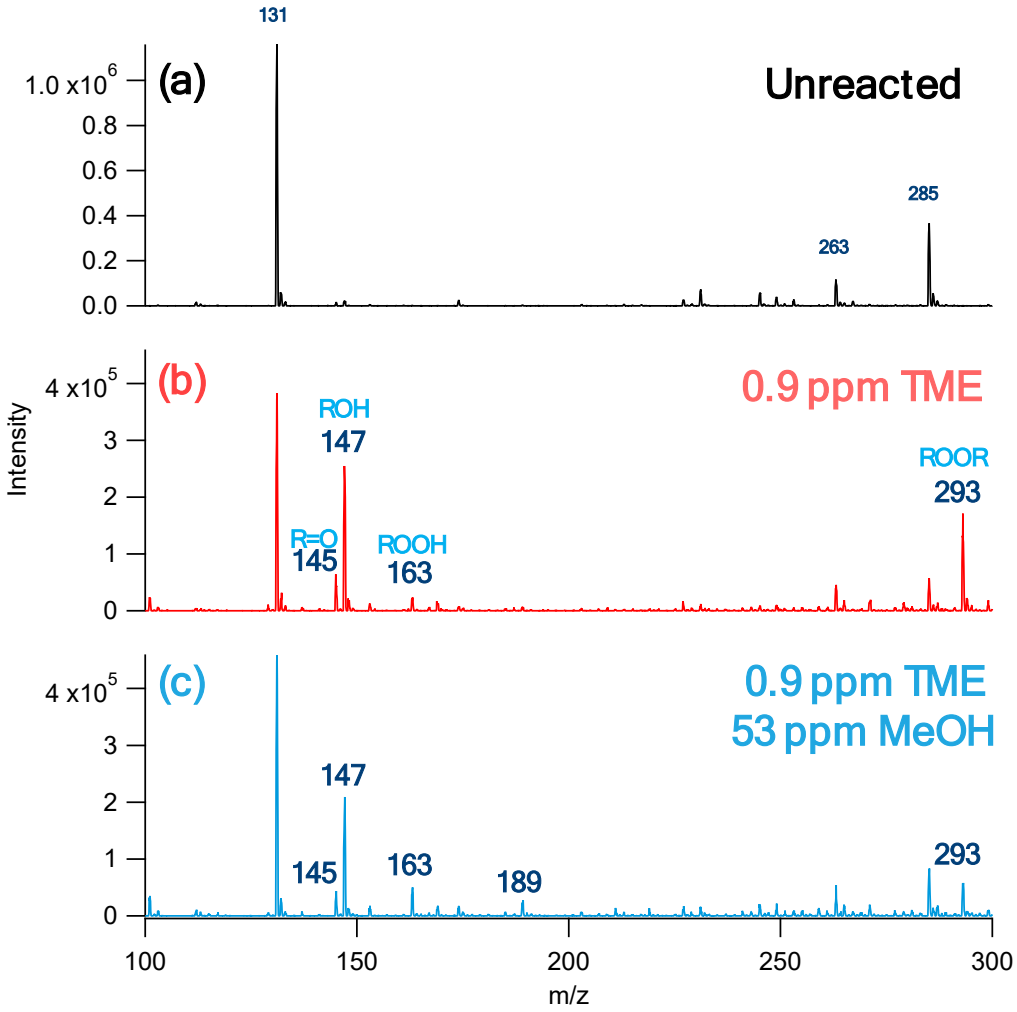

Figure S9. MAIV spectra of GA particles in negative ion mode. Spectra of GA particles **(a)** unreacted; **(b)** reacted with OH radicals, 0.9 ppm TME + 7.5 ppm ozone; **(c)** reacted with OH radicals in the presence of 53 ppm methanol. Numbered labels refer to peaks which correspond either to GA or to its oxidation products, as discussed in the text. Additional peak assignments in negative ion mode: $[GA - H]^-$, *m/z* 131; $[2GA - H]^-$, *m/z* 263; $[2GA + Na - 2H]^-$, *m/z* 285; $[R"(O)OR - H]^-$, *m/z* 189.

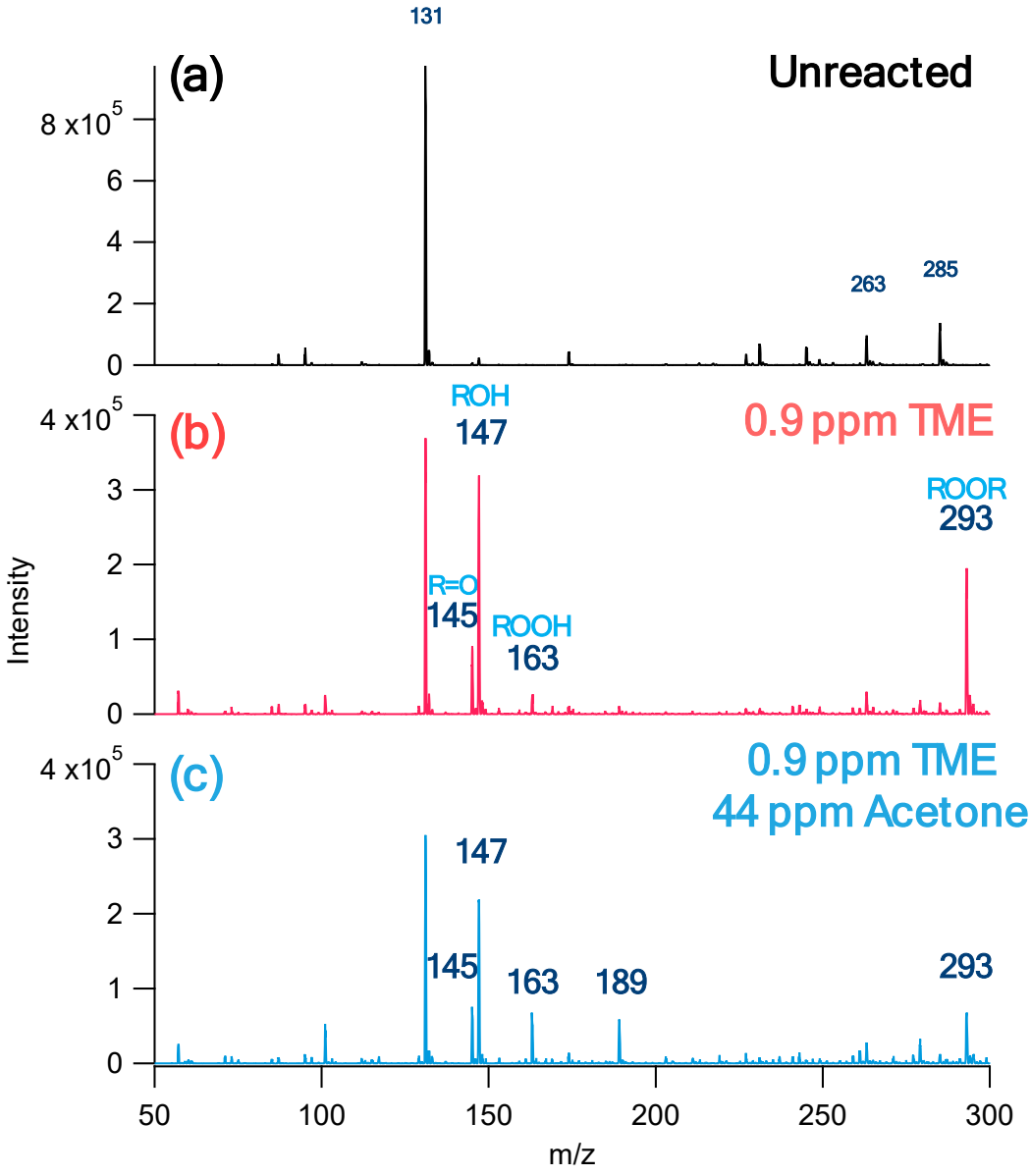

226

227 **Figure S10.** MAIV spectra of GA particles in negative ion mode before and after acetone
228 addition. Spectra of GA particles **(a)** unreacted; **(b)** reacted with OH radicals, 0.9 ppm TME + 7.5
229 ppm ozone; **(c)** reacted with OH radicals in the presence of 44 ppm acetone. $[GA - H]^-$, *m/z* 131;
230 $[2GA - H]^-$, *m/z* 263; $[2GA + Na - 2H]^-$, *m/z* 285; $[R"(O)OR - H]^-$, *m/z* 189.

231

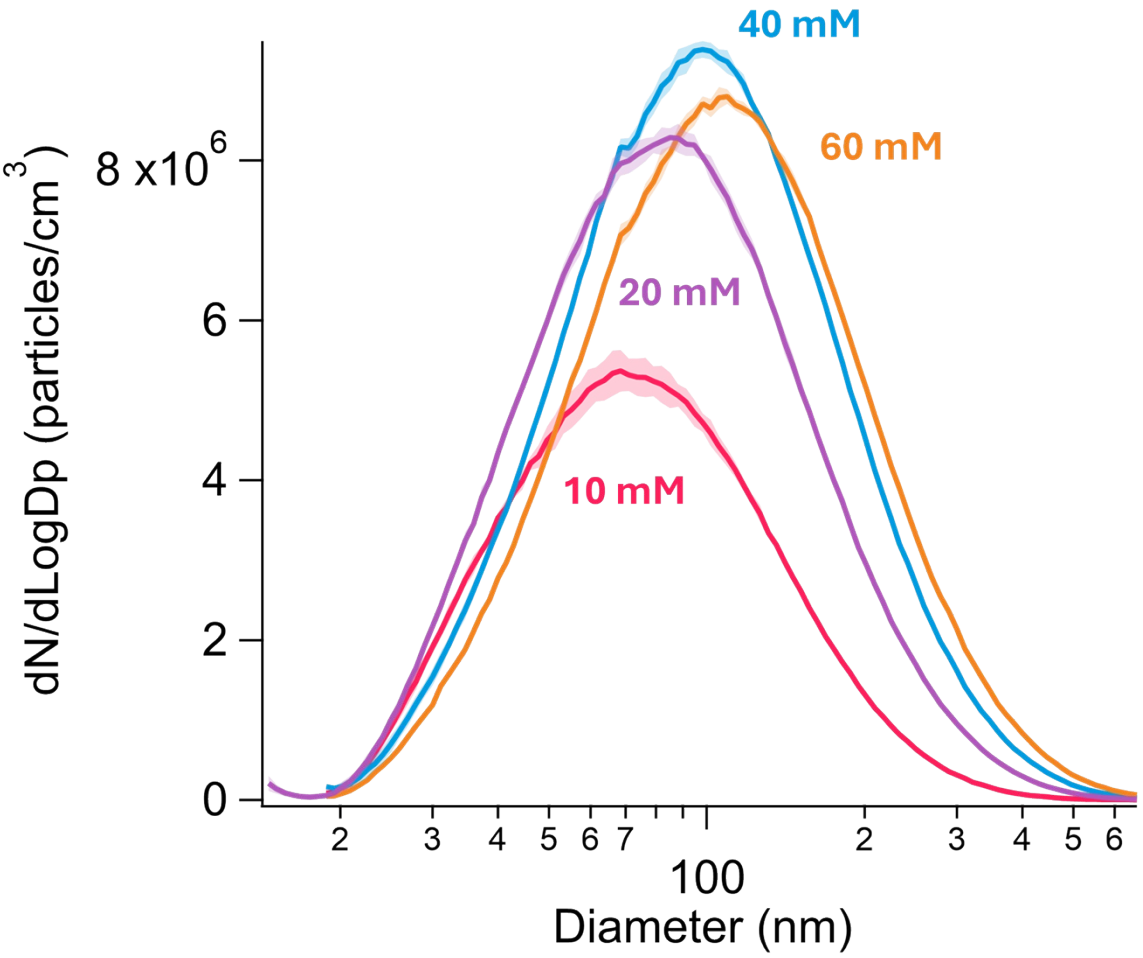

232

233

234 **Figure S11.** Typical size distributions of atomized and dried GA particles as concentration was
235 varied as measured with a scanning mobility particle sizer (SMPS). Each distribution is an average
236 of five scans ± one standard deviation.

237

238

239 **Table S3.** Typical size properties of GA particles measured by the SMPS as the atomized
240 aqueous concentration was varied. Reported values are averages of 5 SMPS scans at each
241 concentration ± one standard deviation.

Atomized GA Concentration (mM)	Mode Diameter (nm)	Number Concentration (#/cm^{-3})	Total Surface Area (nm^2/cm^3)	Surface Area per Particle (SA/N) (nm^2/part)
10	70 ± 4	$(3.47 \pm 0.06) \times 10^6$	$(1.16 \pm 0.02) \times 10^{11}$	$(3.35 \pm 0.08) \times 10^4$
20	86 ± 4	$(5.52 \pm 0.07) \times 10^6$	$(2.48 \pm 0.01) \times 10^{11}$	$(4.49 \pm 0.06) \times 10^4$
40	99 ± 3	$(6.15 \pm 0.07) \times 10^6$	$(3.58 \pm 0.05) \times 10^{11}$	$(5.82 \pm 0.09) \times 10^4$
60	108 ± 2	$(5.92 \pm 0.05) \times 10^6$	$(4.18 \pm 0.04) \times 10^{11}$	$(7.1 \pm 0.1) \times 10^4$

242

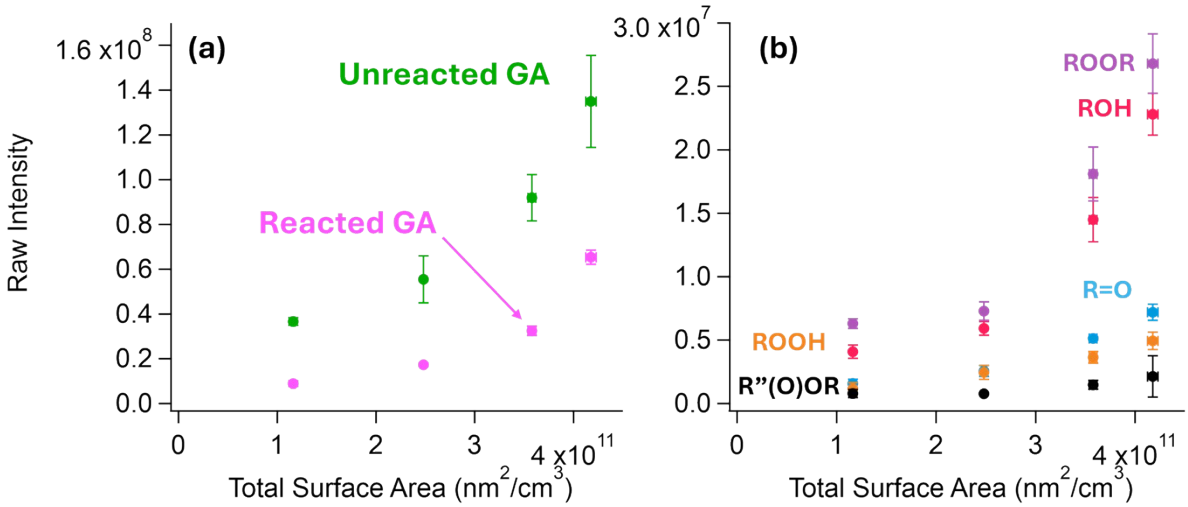

Figure S12. MAIV-MS intensity of (a) GA before and after oxidation and (b) each oxidation product, normalized to the total particle concentration, as function of total GA surface area across size dependence studies. Each species shows a positive trend with surface area. Vertical error bars in intensity are ± one standard deviation from $n = 3$ while horizontal bars from surface area measurements are from $n = 5$.

REFERENCES

1. Jenkin ME, Saunders SM, Pilling MJ. The tropospheric degradation of volatile organic compounds: A protocol for mechanism development. Atmos Environ. 1997;31(1):81-104.
2. Saunders SM, Jenkin ME, Derwent RG, Pilling MJ. Protocol for the development of the master chemical mechanism, MCM v3 (part a): Tropospheric degradation of non-aromatic volatile organic compounds. Atmos Chem Phys. 2003;3(1):161-80.
3. Atkinson R, Baulch DL, Cox RA, Crowley JN, Hampson RF, Hynes RG, et al. Evaluated kinetic and photochemical data for atmospheric chemistry: Volume ii - gas phase reactions of organic species. Atmos Chem Phys. 2006;6:3625-4055.
4. Zuraski K, Grieman FJ, Hui AO, Cowen J, Winiberg FAF, Percival CJ, et al. Acetonyl peroxy and hydroperoxy self- and cross-reactions: Temperature-dependent kinetic parameters, branching fractions, and chaperone effects. J Phys Chem A. 2023;127(37):7772-92.
5. Assali M, Fittschen C. Rate constants and branching ratios for the self-reaction of acetyl peroxy ($CH_3C(O)O_2$) and its reaction with CH_3O_2. Atmosphere. 2022;13(2).
6. Villenave E, Lesclaux R, Seefeld S, Stockwell WR. Kinetics and atmospheric implications of peroxy radical cross reactions involving the $CH_3C(O)O_2$ radical. J Geophys Res-Atmos. 1998;103(D19):25273-85.
7. Atkinson R, Baulch DL, Cox RA, Crowley JN, Hampson RF, Hynes RG, et al. Evaluated kinetic and photochemical data for atmospheric chemistry: Volume i - gas phase reactions of O, HO_x, NO_x and SO_x species. Atmos Chem Phys. 2004;4:1461-738.
8. Jenkin ME, Valorso R, Aumont B, Rickard AR. Estimation of rate coefficients and branching ratios for reactions of organic peroxy radicals for use in automated mechanism construction. Atmos Chem Phys. 2019;19(11):7691-717.
9. Finlayson-Pitts BJ, Pitts JN, Jr. Chemistry of the upper and lower atmosphere - theory, experiments, and applications. San Diego: Academic Press; 2000. 969 p.
10. Qin YM, Perraud V, Finlayson-Pitts BJ, Wingen LM. Peroxides on the surface of organic aerosol particles using matrix-assisted ionization in vacuum (MAIV) mass spectrometry. Environ Sci Technol. 2023;57(38):14260-8.
11. Grossert JS, Fancy PD, White RL. Fragmentation pathways of negative ions produced by electrospray ionization of acyclic dicarboxylic acids and derivatives. Can J Chem. 2005;83(11):1878-90.
12. Peräkylä O, Berndt T, Franzon L, Hasan G, Meder M, Valiev RR, et al. Large gas-phase source of esters and other accretion products in the atmosphere. J Am Chem Soc. 2023;145(14):7780-90.
13. Franzon L, Camredon M, Valorso R, Aumont B, Kurtén T. Ether and ester formation from peroxy radical recombination: A qualitative reaction channel analysis. Atmos Chem Phys. 2024;24(20):11679-99.